European Conference on Optical Communication (ECOC) 2022 © Optica Publishing Group 2022

Probabilistic Constellation Shaping and Subcarrier Multiplexing for Nonlinear Fiber Channels

Junho Cho* and Han Sun

Infinera Corporation, Ottawa, ON, K2K 2X3, Canada, *jcho@infinera.com

Abstract *We show how the symbol rate affects the occurrence of nonlinear interference in systems with finite-length probabilistic constellation shaping. The results suggest that it is necessary to flexibly change the symbol rate according to link parameters and shaping block length to achieve optimal system performance. ©2022 The Author(s)*

Introduction

Probabilistic constellation shaping (PCS) has recently been widely adopted in the optical communications industry due to its advantages of bringing system performance closer to the Shannon limit with a finely adaptable information rate [1-3]. However, as nonlinear interference (NLI) of optical fiber channels is known to be aggravated by PCS [4,5], research is being conducted to solve this problem [6-9]. Approaches to reducing PCS-induced NLI include: *(i)* those based on analytical light propagation theory [4,5] that signals with a smaller kurtosis induce lower NLI, and *(ii)* those based on the empirical findings [8,9] that reducing the block length of some types of PCS algorithms reduces NLI. Rationale to support the latter approach has recently begun to be sought [10]. Interestingly, explanations have emerged that the above two approaches (small kurtosis and short block length) are closely related [11-13]. Namely, although short- and long-block PCS with the same time-averaged signal distribution have the same kurtosis when measured by the conventional method, it has been found that short-block PCS produces smaller kurtosis than long-block PCS when measured after applying a moving average filter to signals [13]. This suggests that the above two approaches can be described integrally.

As empirical evidence accumulates that NLI is reduced by certain types of PCS, research has designed novel PCS algorithms and demonstrated their benefits under selected link conditions. Unfortunately, however, *not* with all symbol rates the modulation formats designed this way are effective. More precisely, there are specific symbol rates that depend on the link parameters at which these modulation formats are most effective in reducing NLI, and if the symbol rates are largely suboptimal, the benefits of these modulation formats can even be completely lost. Therefore, not only do traditional systems that transmit independent and identically distributed (IID) symbols require symbol rate optimization (SRO) [14,15], but PCS systems that transmit statistically correlated symbols also require SRO to maximize system performance. Looking at the recent industry trend that continues to increase the symbol rates as much as the technology allows, this may mean that subcarrier multiplexing should be performed with a variable number of subcarriers.

In this work, we will discuss finite-length PCS and SRO in detail from an NLI perspective.

Windowed Kurtosis

Let $\wp \triangleq \|x\|^2/\langle\|x\|^2\rangle$ be normalized signal power of modulation symbol x, where $\|\cdot\|$ and $\langle\cdot\rangle$ denote Euclidean norm and statistical averaging, respectively. The k-th *windowed standardized central moment* of $\wp$ for $k = 2, 3$ is defined as

$$\bar{m}_k \triangleq \langle(\langle\wp\rangle_w - 1)^k\rangle \cdot (vw)^{k-1}, \tag{1}$$

where $\langle\cdot\rangle_w$ denotes length-w moving average filtering and v is the number of polarizations used for signalling. The moment $\bar{m}_k$ quantifies the k-th order deviation of the signal power $\langle\wp\rangle_w$ measured within a length-w sliding window from the average power (i.e., 1 by definition). If the signal has zero mean, the windowed standardized (non-central) moments $\bar{\mu}_{2k}$ of x (as opposed to $\wp$ in Eq. (1)) can be obtained from $\bar{m}_k$ as

$$\bar{\mu}_4 = \bar{m}_2 + 1, \tag{2}$$

$$\bar{\mu}_6 = \bar{m}_3 + 3\bar{m}_2 + 1. \tag{3}$$

Modulation-dependent NLI is strongly affected by the 4th moment $\bar{\mu}_4$, commonly referred to as *kurtosis*. In general, the greater the kurtosis, the greater the NLI. When $w = 1$, $\bar{\mu}_k$ degenerates to conventional (non-windowed) moments.

Many widely used block-wise PCS algorithms [16-19], either implicitly or explicitly, ensure that the total energy of signals within a shaping block does not exceed a certain value, which is typically much smaller than that of uniform signalling. The block-wise energy constraint creates local energy structures in the light, leading to a decrease in $\bar{\mu}_4$ as w increases, as shown in Fig. 1. In the figure, the dashed lines represent IID symbols, and the solid lines represent finite-length PCS realized by

* Much of this work is based on findings that Junho Cho published while he was at Nokia Bell Labs, Murray Hill, NJ 07733.

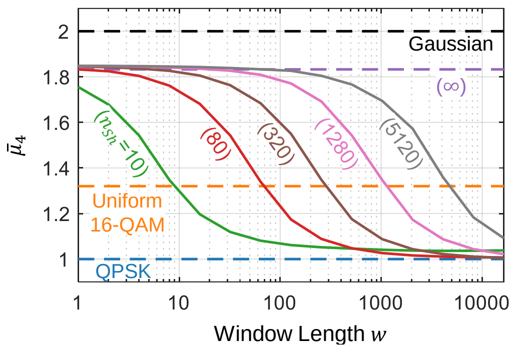

Fig. 1: Windowed kurtosis of IID symbols (dashed lines) and finite-length PCS symbols (solid lines), as a function of the window length.

sphere shaping of 16-ary quadrature amplitude modulation (16-QAM) constellations, with the numbers in the parentheses being shaping block length n_{Sh} in number of *dual-polarization* symbols.

In [12,13], through extensive split-step simulations, it was shown that the amount of self-phase modulation (SPM) and cross-phase modulation (XPM)-induced NLI have the highest correlation with $\bar{\mu}_4$, if $\bar{\mu}_4$ is measured using the window lengths w_{SPM} and w_{XPM} given by

$$w_{SPM} = 2R_{Sym}^2|\beta_2|L_{Span}N_{Span}, \quad (4)$$

$$w_{XPM} = 2R_{Sym}^{3/2}B_{Tot}^{1/2}|\beta_2|L_{Span}N_{Span}, \quad (5)$$

where R_{Sym} is the symbol rate (Bd), β_2 is the fiber dispersion coefficient (s^2/m), L_{Span} is the span length (m), and N_{Span} is the number of spans, assuming ideal Nyquist pulse shaping and uniformly-spaced channels over a total WDM bandwidth of B_{Tot} (Hz). When w_{SPM}, w_{XPM}, and R_{Sym} are all expressed in log scale, they have linear relations as shown in Fig. 2(a) for a standard single-mode fiber (SMF) link with $B_{Tot} = 500$ GHz, $L_{Span} = 100$km, and $N_{Span} = 50$. Given these link parameters, we can redraw $\bar{\mu}_4$ in Fig. 1 as a function of of R_{Sym} using the relations in Eqs. (4)-(5), as shown in Fig. 2(b) (plotted only for w_{SPM}). Figure 2(b) clearly shows that $\bar{\mu}_4$ varies with R_{Sym}, even if all link parameters including transmission distance are fixed.

NLI Due to Interplay of Shaping Block Length and Symbol Rate

For the SMF link above, Fig. 3(a) shows the NLI coefficients η determined by enhanced Gaussian noise (EGN) model analysis [5] on IID symbols. Note that NLI power is proportional to $\eta\langle\|x\|^2\rangle^3$. The figure confirms the findings of [14,15] that the optimal symbol rate R_{Sym}^* for IID symbols is nearly constant regardless of the modulation format, and it is only ~2.1 GBd for this long-haul dispersion-uncompensated link, which is much lower than the symbol rates of optical transceivers being deployed today. We also perform the EGN

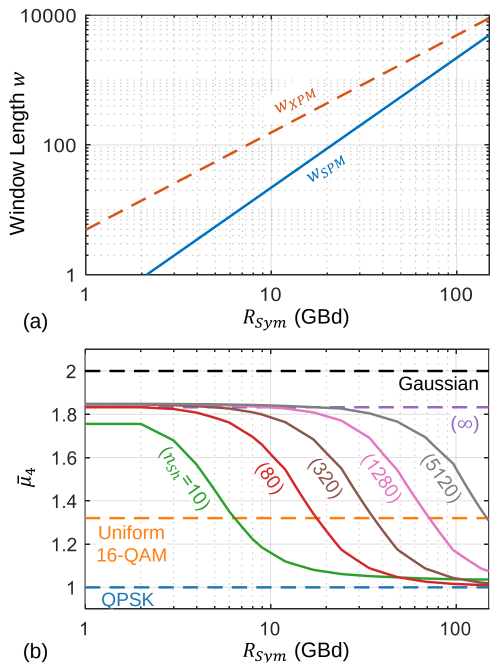

Fig. 2: In 5000km SMF transmission, (a) the window length for measuring windowed kurtosis depends on R_{Sym}, and (b) using this window length, the windowed kurtosis in Fig. 1 is expressed as a function of R_{Sym}.

model analysis on sphere-shaped symbols, as shown in the solid lines in Fig. 3(b). Here, we replace non-windowed μ_4 and μ_6 with windowed $\bar{\mu}_4$ and $\bar{\mu}_6$, since it was shown [12,13] that this allows the EGN model to produce NLI predictions in much better agreement with the split-step simulation results. From the figure, the followings can be observed:

i) Compared to IID PCS ($n_{Sh} = \infty$, purple dashed line), a short block length $n_{Sh} = 10$ (green solid line) significantly reduces NLI.

ii) The benefit of the short block length $n_{Sh} = 10$ is greatest when $R_{Sym}^* \approx 5$ GBd, but gradually diminishes as R_{Sym} departs away from R_{Sym}^*.

iii) As the shaping block length n_{Sh} increases, the benefit of NLI mitigation due to PCS decreases, and the NLI-minimizing R_{Sym}^* increases.

To better illustrate the point *iii* above, we plot in Fig. 3(c) the trajectory of NLI-minimizing R_{Sym}^* when n_{Sh} increases. In the sense that quadrature phase shift-keying (QPSK) represents the limit of reducing the PCS block length (cf. see Fig. 2(b) where a decrease in n_{Sh} makes the windowed kurtosis $\bar{\mu}_4$ converge faster to the minimum given by QPSK), R_{Sym}^* starts from 2.1 GBd of QPSK (blue dashed line). As n_{Sh} increases, a higher R_{Sym} is required to make $\bar{\mu}_4$ small (cf. Fig. 2(b)), but at this high R_{Sym}, the lower bound of the NLI coefficient determined by QPSK is higher than that achieved at R_{Sym}^* (cf. Fig. 3(b)), and the NLI coefficient produced by PCS only goes down near this "raised" lower bound. Therefore, at high

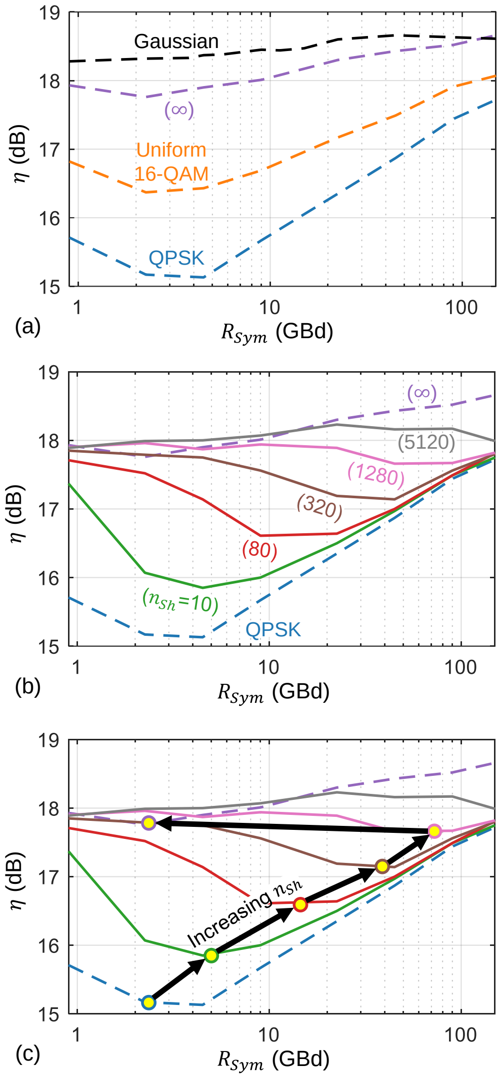

Fig. 3: (a) NLI coefficient η of various IID symbols, evaluated for 5000km SMF transmission with $B_{Tot} = 500$ GHz, (b) those of sphere-shaped symbols with block length n_{Sh} (numbers in the parentheses), and (c) the trajectory of NLI-minimizing R^*_{Sym} when n_{Sh} increases.

symbol rates above 100 GBd, although the windowed kurtosis $\bar{\mu}_4$ is nearly the theoretical minimum for all shaping block lengths n_{Sh} of practical interest, the effect of small $\bar{\mu}_4$ in reducing NLI vanishes due to excessively suboptimal R_{Sym}.

If we ignore the rise of the lower bound of η due to suboptimal R_{Sym} and only consider the aspect of $\bar{\mu}_4$, the symbol rate $R^{\dagger}_{Sym}$ that makes the window lengths w_{SPM} and w_{XPM} equal to the shaping block length n_{Sh} can be obtained by plugging $w_{SPM} = n_{Sh}$ and $w_{XPM} = n_{Sh}$ into Eqs. (4) and (5) as

$$R^{\dagger}_{Sym,SPM} = \left[n_{Sh}/(2|\beta_2|L_{Span}N_{Span})\right]^{1/2}, \quad (6)$$

$$R^{\dagger}_{Sym,XPM} = \left[n_{Sh}/(2|\beta_2|B_{Tot}^{1/2}L_{Span}N_{Span})\right]^{2/3}, \quad (7)$$

as shown in Fig. 4 as a function of the transmission distance $L_{Span}N_{Span}$ for SMF fiber. Note that when $n_{Sh} = 1$, Eq. (6) is very close to the optimal symbol

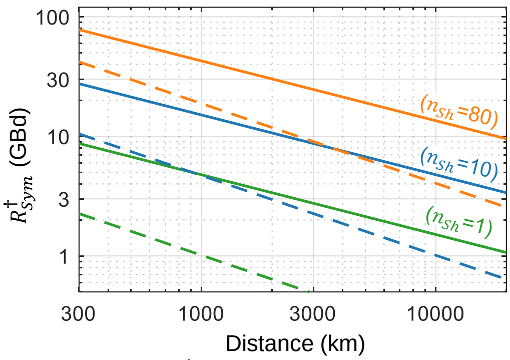

Fig. 4: Symbol rates $R^{\dagger}_{Sym}$ to achieve $w_{SPM} = n_{Sh}$ (solid lines) and $w_{XPM} = n_{Sh}$(dashed lines) in SMF fiber, when $B_{Tot} =$ 500 GHz.

rate formula of IID symbols given in [15]. Figure 4 shows that as n_{Sh} increases or trans-mission distance decreases, the symbol rates to achieve $w_{SPM} = n_{Sh}$ and $w_{XPM} = n_{Sh}$ increase, which is consistent with Fig. 3(c) until the rise of the lower bound of η due to suboptimal R_{Sym} comes into play.

Linear Channel Considerations

We have discussed the intricate interplay of shaping block length and symbol rate, focusing on the NLI induced by the Kerr effect. In practice, however, most systems operate at an optimal launch power where the linear noise power is about twice the NLI power. The linear channel noise includes amplified spontaneous emission (ASE) noise accumulating through erbium-doped fiber amplifiers (EDFAs), thermal noise of radio frequency (RF) amplifiers and transimpedance amplifiers (TIAs), and is often modelled as additive white Gaussian noise (AWGN). Unlike under NLI, maximizing system performance under AWGN requires that the shaping block length be chosen as long as possible [1], as has already been approached fairly closely with commercial trans-ceivers in real networks [3]. Future PCS systems must now evolve toward adequately addressing the question of nonlinearity.

Conclusion

The NLI power in finite-length PCS systems is determined by the complex interaction of the symbol rate and the statistical properties of modulated signal. Studies suggest that the symbol rate needs to be flexibly changed, e.g., through software configurable subcarrier multi-plexing, to tailor the system to the underlying nonlinear channel conditions. However, it is in our view that significant innovation is needed to reduce the implementation complexity of such systems. Electrical power efficiency and cost-per-bit of the overall system are also important practical metrics that should be weighed in.

References

[1] G. D. Forney and L.-F. Wei, “Multidimensional constellations. I. Introduction, figures of merit, and generalized cross constellations,” *IEEE Journal on Selected Areas in Communications*, vol. 7, no. 6, pp. 877–892, Aug. 1989.

[2] J. Cho and P. J. Winzer, “Probabilistic constellation shaping for optical fiber communications,” *Journal of Lightwave Technology*, vol. 37, no. 6, pp. 1590–1607, Mar. 2019.

[3] H. Sun et al., “800G DSP ASIC design using probabilistic shaping and digital sub-carrier multiplexing,” *Journal of Lightwave Technology*, vol. 38, no. 17, pp. 4744–4756, Sep. 2020.

[4] R. Dar et al., Properties of nonlinear noise in long, dispersion-uncompensated fiber links,” *Optics Express*, vol. 21, no. 22, pp. 25685–25699, Nov. 2013.

[5] A. Carena et al., “EGN model of non-linear fiber propagation,” *Optics Express*, vol. 22, no. 13, pp. 16335–16362, Jun. 2014.

[6] J. Cho et al., “Low-complexity shaping for enhanced nonlinearity tolerance,” in *Proc. European Conference on Optical Communications (ECOC)*, Dusseldorf, Germany, Sep. 2016, pp. 1–3.

[7] Y. C. Gültekin et al., “Kurtosis-limited sphere shaping for nonlinear interference noise reduction in optical channels,” *Journal of Lightwave Technology*, vol. 40, no. 1, pp. 101–112, Jan. 2022.

[8] A. Amari et al., “Introducing enumerative sphere shaping for optical communication systems with short blocklengths,” *Journal of Lightwave Technology*, vol. 37, no. 23, pp. 5926–5936, Dec. 2019.

[9] T. Fehenberger et al., “Analysis of nonlinear fiber interactions for finite-length constant-composition sequences,” *Journal of Lightwave Technology*, vol. 38, no. 2, pp. 457–465, Jan. 2020.

[10] R. R. Borujeny and F. Kschischang. “Why constant-composition codes reduce nonlinear interference noise,” Mar. 2022, arXiv:2203.02641.

[11] K. Wu et al., “Temporal energy analysis of symbol sequences for fiber nonlinear interference modelling via energy dispersion index,” *Journal of Lightwave Technology*, vol. 39, no. 18, pp. 5766–5782, Sep. 2021.

[12] J. Cho et al., “Shaping lightwaves in time and frequency for optical fiber communication,” *Nature Communications*, vol. 13, no. 1, pp. 1–11, Feb. 2022.

[13] J. Cho and R. Tkach, “On the kurtosis of modulation formats for characterizing the nonlinear fiber propagation,” *Journal of Lightwave Technology*, vol. 40, no. 12, pp. 3739–3748, Jun. 2022.

[14] P. Poggiolini et al., “A simple and effective closed-form GN model correction formula accounting for signal non-Gaussian distribution,” *Journal of Lightwave Technology*, vol. 33, no. 2, pp. 459–473, Jan. 2015.

[15] P. Poggiolini et al., “Analytical and experimental results on system maximum reach increase through symbol rate optimization,” *Journal of Lightwave Technology*, vol. 34, no. 8, pp. 1872–1885, Apr. 2016.

[16] T. V. Ramabadran, “A coding scheme for m-out-of-n codes,” *IEEE Transactions on Communications*, vol. 38, no. 8, pp. 1156–1163, Aug. 1990.

[17] F. M. J.Willems and J. J.Wuijts, “A pragmatic approach to shaped coded modulation,” in *Proc. IEEE 1st Symposium on Communications and Vehicular Technology in the Benelux (SCVT)*, 1993, pp. 1–6.

[18] J. Cho, “Prefix-free code distribution matching for probabilistic constellation shaping,” *IEEE Transactions on Communications*, vol. 68, no. 2, pp. 670–682, Feb. 2020.

[19] T. Yoshida, M. Karlsson and E. Agrell, “Hierarchical distribution matching for probabilistically shaped coded modulation,” *Journal of Lightwave Technology*, vol. 37, no. 6, pp. 1579–1589, Mar. 2019.